

Collective Flavor Oscillations Of Supernova Neutrinos and r-Process Nucleosynthesis

Sovan Chakraborty^{*,a}, Sandhya Choubey^{†,b}, Srubabati Goswami^{‡,c}, Kamales Kar^{*,d}

**Saha Institute of Nuclear Physics,
1/AF Bidhannagar, Kolkata 700064, India*

*†Harish-Chandra Research Institute,
Chhatnag Road, Jhansi, Allahabad 211019, India*

*‡Physical Research Laboratory, Navrangpura,
Ahmedabad 380009, India*

ABSTRACT

Neutrino-neutrino interactions inside core-collapse supernovae may give rise to flavor oscillations resulting into collective swap of flavors. These oscillations depend on the initial energy spectra and initial relative fluxes or initial luminosities of the neutrinos. It has been observed that departure from energy equipartition among different flavors can give rise to one or more sharp spectral swap over energy termed as splits. We study the occurrence of splits in the neutrino and antineutrino spectra varying the initial relative fluxes for different models of initial energy spectrum in both normal and inverted hierarchy. These initial relative flux variations give rise to several possible split patterns where as variation over different models of energy spectra give similar results. We explore the effect of these spectral splits on the electron fraction, Y_e , that governs r-process nucleosynthesis inside supernovae. Assuming the condition $Y_e < 0.5$, needed for successful r-process nucleosynthesis we present exclusion plots of the initial luminosities or relative fluxes, including the effect of collective oscillations.

^a email: sovan.chakraborty@saha.ac.in

^b email: sandhya@hri.res.in

^c email: sruba@prl.res.in

^d email: kamales.kar@saha.ac.in

1 Introduction

Neutrinos from a core-collapse supernova can play an important role in probing both neutrino properties as well as throwing light on the supernova mechanism [1, 2]. Neutrinos emitted during the explosion of core-collapse supernovae (SN) pass through very large density variation of matter and can undergo MSW resonant flavor conversion [3] which can give useful information on neutrino mass hierarchy and the third leptonic mixing angle θ_{13} . They are also influenced by the shock wave formed in the SN core and thus carry information about the explosion mechanism [4, 5, 6, 7].

Recently it was realized that a crucial feature in the study of SN neutrinos comes from the collective neutrino-neutrino interaction at very high densities of the core and this may change the emitted flux of different flavors substantially [10]-[42]. The phenomenology of supernova neutrinos with collective effect including Earth matter effect on SN neutrinos [35], prompt SN [31, 32], Diffuse Neutrino background from SN [43], failed SN [44] as well as CP violation in SN neutrinos [38] has been studied. For a recent review we refer to [45].

It has been shown that effectively the collective evolution of a three-flavor $(\nu_e, \nu_\mu, \nu_\tau)$ system can be treated like a two flavor (ν_e, ν_x) scenerio, where ν_x can be ν_μ or ν_τ or a linear combination of ν_μ and ν_τ [33, 40]. The flavor evolution for this system is driven by the effective mass squared difference Δm^2 and the mixing angle θ_{13} . This two flavor scenerio which has been extensively studied [20, 25, 26, 29] shows that for inverted hierarchy (IH, $\Delta m^2 < 0$), above a critical energy (split energy E_c), the spectrum in both the electron neutrino (ν_e) and antineutrino ($\bar{\nu}_e$) sectors end up with a complete exchange or swap with ν_x and $\bar{\nu}_x$ respectively, this is referred as “spectral swap”. Recently the studies in [41, 42] analyzed the role of equipartition in energy and variation of luminosity and showed the interesting possibility of multiple splits in the supernova neutrino spectrum for IH. Single spectral split for Normal Hierarchy (NH, $\Delta m^2 > 0$) was also reported for certain values of luminosities.

In this paper our goal is to study (a) the impact of spectral splits on the electron fraction (Y_e) which is a diagnostic of successful r-process nucleosynthesis in supernova and (b) the inverse problem which is to see if it is possible to put any constraint on the luminosities by demanding the neutron rich condition on Y_e which is required for synthesis of heavy nuclei.

Though the site for r-process nucleosynthesis is not known definitely, supernovae are considered to be excellent candidates for it. One of the criteria for the rapid nucleosynthesis to take place is that it has to be in a neutron-rich region. With the two competing beta processes $n + \nu_e \rightarrow p + e^-$ and $p + \bar{\nu}_e \rightarrow n + e^+$ occurring in the hot bubble and neutrino driven wind region, the minimal condition is that the electron fraction, $Y_e < 0.5$. A more realistic constraint may be $Y_e < 0.45$.

The effect of the collective oscillations on the possibility of getting n-rich region in the hot bubble was studied in [13]. The problem of r-process in the neutrino-wind region with different evolution scenarios was looked into in [46]. With an improved understanding of the spectral splits in the collective oscillations [41, 42], we re-examine the problem of SN r-process using the two flavor basis as mentioned above. It is worth mentioning here that r-process occurs at a distance where the usual MSW effects are absent. Therefore the conclusions drawn from considerations of r-process are purely from the effect of collective oscillations. We consider different models for the initial neutrino spectrum with different hierarchies among average energies and departures from energy equipartition among flavors. We demonstrate the occurrence of spectral splits due to these variations on the probabilities and the fluxes for both hierarchies. We use the constraint that the

environment should be neutrino rich for successful r-process and delineate the resulting constraints that are obtained on the fractional luminosities. The paper is organized as follows. In Section 2, we outline the neutrino-neutrino interaction in the context of the supernova problem. First the two flavor evolution equations are presented. Next we vary the fractional luminosities for different initial energy spectrum model and study the effect of collective oscillations, especially the effect of the spectral splits on the emitted neutrino flux. In Section 3, we discuss how the evolution of the electron fraction Y_e is affected by collective oscillations. The value of Y_e determines the possibility of having r-process nucleosynthesis in the supernova environment. We impose the constraint that the environment should be neutron rich and study the initial relative fluxes or relative luminosities which are allowed under this constraint. Finally Section 4 makes some concluding remarks.

2 Two flavor neutrino-neutrino interaction and Supernova

Close to the neutrinosphere, due to the large neutrino density, neutrinos form a background to themselves. This neutrino-neutrino interaction effect is nonlinear and can give rise to collective flavor transition of neutrinos and antineutrinos. In this section we discuss the flavor evolution equations, different models of supernova neutrino spectrum and the impact of the collective effects on the probabilities and the fluxes for both NH and IH.

2.1 Two flavor evolution equations of SN Neutrinos

Due to the large neutrino density inside the neutrinosphere, the neutrino-neutrino interactions lead to coherent oscillations of neutrinos of different energies with some average frequency, giving rise to synchronized oscillations. However, there is no effective flavor conversion due to these synchronized oscillations as the effective mixing angle is highly suppressed due to the large MSW potential in the region close to the neutrinosphere. With the neutrino density decreasing outward, bipolar oscillations begin to take place. These oscillations can lead to complete or partial swapping (spectral split) of the $\bar{\nu}_e$ (ν_e) and $\bar{\nu}_x$ (ν_x) spectra depending on their initial luminosities and average energies. Finally, after a few hundred kilometers, the neutrino-neutrino interactions become negligible and it is the MSW transitions which dominate.

As shown in [33, 40] the collective effect due to neutrino-neutrino interaction effectively involves only two flavors of neutrinos (ν_e, ν_x), while the other flavor (ν_y) does not evolve under this collective potential. Here ν_x is a linear combination of ν_μ, ν_τ and ν_y is the orthogonal combination to ν_x . The only way ν_y can effect the final neutrino spectrum is by MSW transition which happens at a larger radius of about 10^{4-5} km, well beyond the collective region which is within a few hundred km from the center of the exploding star. Therefore, the effective evolution of the neutrinos is very well described by the two flavor formalism.

The evolution equations in the two-family Bloch vector notation for the polarization vectors of the neutrino (\mathbf{P}) and antineutrino (\mathbf{P}') sector, in the ‘‘single angle approximation’’ [20], are,

$$\dot{\mathbf{P}} = \mathbf{P} \times (\omega\mathbf{B} - \lambda\hat{\mathbf{z}} - \mu\mathbf{D}) , \quad (1)$$

$$\dot{\mathbf{P}}' = \mathbf{P}' \times (-\omega\mathbf{B} - \lambda\hat{\mathbf{z}} - \mu\mathbf{D}) , \quad (2)$$

where the terms involving ω , λ and μ are the ones having the vacuum, matter and neutrino-neutrino interaction effects and the frequencies are represented by

$$\mathbf{B} = (-\sin 2\theta, 0, \cos 2\theta)^T, \quad \omega = \frac{\Delta m^2}{2E}, \quad (3)$$

$$\hat{\mathbf{z}} = (0, 0, 1)^T, \quad \lambda = \sqrt{2}G_F N_e, \quad (4)$$

$$\mathbf{D} = \frac{1}{(N_{\nu_e} + N_{\nu_x} + N_{\bar{\nu}_e} + N_{\bar{\nu}_x})} \int dE (n\mathbf{P} - \bar{n}\mathbf{P}') \quad , \quad \mu = \sqrt{2}G_F(N_{\nu_e} + N_{\nu_x} + N_{\bar{\nu}_e} + N_{\bar{\nu}_x}), \quad (5)$$

respectively. As usual, θ and Δm^2 are the mixing angle and mass squared difference respectively. In what follows θ_{eff} is taken as 10^{-5} and $|\Delta m^2| = |\Delta m_{31}^2| = |m_3^2 - m_1^2| = 3 \times 10^{-3} \text{ eV}^2$. N_α 's represent the total effective number density of the α th species.

$$N_\alpha = \int dE n_\alpha, \quad (6)$$

where,

$$n = n_{\nu_e} + n_{\nu_x}, \quad \bar{n} = n_{\bar{\nu}_e} + n_{\bar{\nu}_x}, \quad (7)$$

n_α 's are the effective number density per unit energy for the α 'th species of neutrino and can be expressed as [20]

$$n_\alpha(r, E) = \frac{D(r)}{2\pi R_\alpha^2} \frac{L_\alpha}{\langle E_\alpha \rangle} \Psi_\alpha(E), \quad (8)$$

where L_α and $\langle E_\alpha \rangle$ are the luminosity and average energy for the α th (anti)neutrino species, R_α is the neutrinosphere radius, and $D(r)$ denotes the geometrical function in the single angle approximation [20] and can be expressed as,

$$D(r) = \frac{1}{2} \left(1 - \sqrt{1 - \left(\frac{R_\alpha}{r} \right)^2} \right)^2. \quad (9)$$

The initial flux of the α th species at the neutrinosphere is given by $\frac{L_\alpha}{\langle E_\alpha \rangle}$ whereas the initial energy distribution is represented by $\Psi_\alpha(E)$.

The matter effect is removed from the evolution equations as the equations are considered in a frame rotating with angular velocity $-\lambda\mathbf{z}$ [19]. In such a frame all the physical observables remain the same. Thus the evolution equations are

$$\dot{\mathbf{P}} = \mathbf{P} \times (\omega\mathbf{B} - \mu\mathbf{D}), \quad (10)$$

$$\dot{\mathbf{P}}' = \mathbf{P}' \times (-\omega\mathbf{B} - \mu\mathbf{D}). \quad (11)$$

These are nonlinear coupled equations (due to the 2nd term containing \mathbf{D}) and have to be solved numerically.

Note that though the matter potential is mostly rotated away, it may become crucial in the evolution in some cases [21, 29, 30, 36, 2]. In the subsequent discussions we assume that such effects are negligible, as without this assumption the numerical calculations become very time consuming. It is evident from the evolution Eqs. (10) and (11) that there are two relevant frequencies, the usual vacuum frequency (ω) and the neutrino-neutrino interaction strength parameter (μ). For our chosen Δm^2 the vacuum frequency is

$$\omega = \frac{\Delta m^2}{2E} = \frac{30}{(4E/MeV)} \text{ km}^{-1}. \quad (12)$$

The usual SN neutrino energy considered is in the range of 0 to 50 MeV, as the SN neutrino flux beyond 50 MeV is very small. Hence we use neutrino energy upto 50 MeV for our calculation.

The other frequency (μ) representing neutrino-neutrino interaction is nontrivial, and is given by

$$\mu = \sqrt{2}G_F(N_{\nu_e} + N_{\nu_x} + N_{\bar{\nu}_e} + N_{\bar{\nu}_x}). \quad (13)$$

The Eqs. (6) to (9) imply that contribution of the α -th species to μ is dependent on radial distance (r), neutrinosphere radius (R_α), initial flux ($\frac{L_\alpha}{(E_\alpha)}$) and initial energy distribution ($\Psi_\alpha(E)$). In our analysis, neutrinosphere radius is taken as 10 km whereas other inputs like initial flux and energy distribution depend on the choice of initial neutrino spectrum model. We analyze the evolution for several neutrino spectrum model.

2.2 Models of Initial Neutrino Spectrum

In a core-collapse SN, the gravitational binding energy (about a few times 10^{53} ergs) is converted to neutrinos and antineutrinos with energies of the order of 10 MeV and gets emitted in the subsequent ~ 10 sec. Initially a neutronization burst comes out consisting of pure ν_e s but with only a very small fraction of the total energy and after that the thermal neutrinos and antineutrinos of all three flavors are emitted. For the thermal neutrinos the initial energy distribution is expected to be Fermi-Dirac (FD), but the results of several simulations [47, 48, 49] found that the distribution must be close to pinched thermal spectra [49] i.e. with a deficit on the high energy side compared to FD. Fermi-Dirac(FD) distribution in energy implies

$$\Psi_\alpha^{FD}(E) \propto \frac{\beta_\alpha (\beta_\alpha E)^2}{e^{\beta_\alpha E} + 1}, \quad (14)$$

and for a choice of average energies of different flavors

$$\langle E_{\nu_e} \rangle = 10 \text{ MeV}, \quad \langle E_{\bar{\nu}_e} \rangle = 15 \text{ MeV}, \quad \langle E_{\nu_x} \rangle = \langle E_{\bar{\nu}_x} \rangle = 24 \text{ MeV}, \quad (15)$$

the inverse temperature parameters are [29]

$$\beta_{\nu_e} = 0.315 \text{ MeV}^{-1}, \quad \beta_{\bar{\nu}_e} = 0.210 \text{ MeV}^{-1}, \quad \beta_{\nu_x} = \beta_{\bar{\nu}_x} = 0.131 \text{ MeV}^{-1}. \quad (16)$$

Whereas the pinched spectra for different simulations are parameterized as [49]

$$\Psi_\alpha(E) = \frac{(1 + \zeta_\alpha)^{1+\zeta_\alpha}}{\Gamma(1 + \zeta_\alpha)} \left(\frac{E_\alpha}{\langle E_\alpha \rangle} \right)^{\zeta_\alpha} \frac{\exp\left(- (1 + \zeta_\alpha) \frac{E_\alpha}{\langle E_\alpha \rangle}\right)}{\langle E_\alpha \rangle}, \quad (17)$$

$\langle E_\alpha \rangle$ is the average energy of ν_α , and ζ_α is the pinching parameter.

The effective number density for the α th species per unit energy is given by

$$n_\alpha(r, E) = \frac{D(r)}{2\pi R_\alpha^2} \frac{L_\alpha}{\langle E_\alpha \rangle} \Psi_\alpha(E). \quad (18)$$

For a specific choice of $\Psi_\alpha(E)$ the initial flux ($\phi_\alpha = \frac{L_\alpha}{\langle E_\alpha \rangle}$) for the α th flavor need to be specified and are very crucial input parameters in our study. Supernova models tell us that almost all the gravitational energy released in core collapse supernovae comes out as $\nu\bar{\nu}$ s of all flavors. Only one or two percent of it goes into the explosion and the electromagnetic radiation emitted in all wavelengths. Thus the total SN binding energy released ($E_B = 3 \times 10^{53}$ erg) is related to the individual flavor luminosities by

$$L_{\nu_e} + L_{\bar{\nu}_e} + 4L_{\nu_x} = \frac{E_B}{\tau}, \quad (19)$$

assuming no distinction between ν_x and $\bar{\nu}_x$. We also assume a time-independent constant luminosity over the time τ . We take $\tau = 10$ seconds. Thus the initial fluxes of different flavors get constrained by

$$\phi_{\nu_e}^0 \langle E_{\nu_e} \rangle + \phi_{\bar{\nu}_e}^0 \langle E_{\bar{\nu}_e} \rangle + 4\phi_{\nu_x}^0 \langle E_{\nu_x} \rangle = 3 \times 10^{52}. \quad (20)$$

If we denote the ratio between the initial fluxes of different flavors by

$$\phi_{\nu_e}^0 : \phi_{\bar{\nu}_e}^0 : \phi_{\nu_x}^0 = \phi_{\nu_e}^r : \phi_{\bar{\nu}_e}^r : 1, \quad (21)$$

where $\phi_{\nu_e}^r, \phi_{\bar{\nu}_e}^r$ are positive numbers, then Eq. (20) can be written as

$$\phi_{\nu_x}^0 (\phi_{\nu_e}^r \langle E_{\nu_e} \rangle + \phi_{\bar{\nu}_e}^r \langle E_{\bar{\nu}_e} \rangle + 4\langle E_{\nu_x} \rangle) = 3 \times 10^{52}. \quad (22)$$

Note that $\phi_{\nu_e}^r = \frac{\phi_{\nu_e}^0}{\phi_{\nu_x}^0}$, $\phi_{\bar{\nu}_e}^r = \frac{\phi_{\bar{\nu}_e}^0}{\phi_{\nu_x}^0}$ are basically initial relative fluxes. Thus different choices of $\phi_{\nu_e}^r$ and $\phi_{\bar{\nu}_e}^r$ imply different relative luminosities or relative fluxes.

Four representative sets for the energy spectra (in terms of $\langle E_\alpha \rangle$ and the pinching factor ζ_ν) and flux ratios usually discussed in literature, are given in Table 1. One simulation by the Lawrence Livermore group (LL) [47] and two different simulations by the Garching group (G1, G2) [49] are presented. Recently [41] used another set of ‘‘plausible’’ flux parameters giving rise to multiple splits in the neutrino spectra is also given. We call this ‘G3’. For the LL spectra we use the FD distribution for Ψ given in Eq. (14). The β_α for LL are given in Eq. (16). For G1, G2 and G3 spectra we use the pinched spectrum defined in Eq. (17). We assume $\zeta_{\nu_x} = \zeta_{\bar{\nu}_x} = 4$ and $\zeta_{\nu_e} = \zeta_{\bar{\nu}_e} = 3$ for G1 and G2. For G3 all $\zeta_\alpha = 3$.

Model	$\langle E_{\nu_e} \rangle$	$\langle E_{\bar{\nu}_e} \rangle$	$\langle E_{\nu_x, \bar{\nu}_x} \rangle$	$\phi_{\nu_e}^r = \frac{\phi_{\nu_e}^0}{\phi_{\nu_x}^0}$	$\phi_{\bar{\nu}_e}^r = \frac{\phi_{\bar{\nu}_e}^0}{\phi_{\nu_x}^0}$
LL	12	15	24	2.00	1.60
G1	12	15	18	0.80	0.80
G2	12	15	15	0.50	0.50
G3	12	15	18	0.85	0.75

Table 1: The parameters of the used primary neutrino spectra models motivated from SN simulations of the Garching (G1, G2) and the Lawrence Livermore (LL) group. We assume $\zeta_{\nu_x} = \zeta_{\bar{\nu}_x} = 4$ and $\zeta_{\nu_e} = \zeta_{\bar{\nu}_e} = 3$ for G1 and G2. For G3 all $\zeta_\alpha = 3$. For LL we use a pure FD spectrum.

Note that the LL simulation obtained a large hierarchy $\langle E_{\nu_e} \rangle < \langle E_{\bar{\nu}_e} \rangle < \langle E_{\nu_x} \rangle \approx \langle E_{\bar{\nu}_x} \rangle$, and an almost complete equipartition of energy among the flavors. The Garching simulations predict a smaller hierarchy between the average energies, incomplete equipartition, and increased spectral pinching. The differences in the values of these parameters arise from the different physics inputs. The equipartition of energy implies

$$L_{\nu_e} = L_{\bar{\nu}_e} = L_{\nu_x} . \quad (23)$$

In terms of our notation it means

$$\phi_{\nu_e}^r = \frac{\langle E_{\nu_x} \rangle}{\langle E_{\nu_e} \rangle}; \quad \phi_{\bar{\nu}_e}^r = \frac{\langle E_{\nu_x} \rangle}{\langle E_{\bar{\nu}_e} \rangle} . \quad (24)$$

So complete equipartition for the Garching simulations would imply flux ratios (Table 2) different from the values in Table 1. Recent analyses [42] have shown that the multiple split cases have origin in the departure from energy equipartition.

Actually there is no reason that equipartition should be strictly followed for the energy released

Model	$\phi_{\nu_e}^r = \frac{\phi_{\nu_e}^0}{\phi_{\nu_x}^0}$	$\phi_{\bar{\nu}_e}^r = \frac{\phi_{\bar{\nu}_e}^0}{\phi_{\nu_x}^0}$
G1	1.50	1.20
G2	1.25	1.00
G3	1.50	1.20

Table 2: The flux ratios for the Garching models with equipartition of energy

from a real supernova. In the next subsection we make extensive analysis of this multiple split phenomena with varying initial fluxes, which is equivalent to varying $\phi_{\nu_e}^r$ and $\phi_{\bar{\nu}_e}^r$.

2.3 Survival Probability and Flux

As stated above in this subsection we discuss the impact due to the variation of initial relative fluxes ($\phi_{\nu_e}^r$ and $\phi_{\bar{\nu}_e}^r$) on the final spectrum. The final spectrum is calculated at 400 km as collective

effect is expected to vanish at around 400 km. We also analyze this effect for different models of initial neutrino spectrum LL, G1 and G3.

In principle the values of $\phi_{\nu_e}^r$ and $\phi_{\bar{\nu}_e}^r$ can lie in a large range. Thus analysing this variation would require study in a wide range of the $\phi_{\nu_e}^r$ - $\phi_{\bar{\nu}_e}^r$ parameter space. Instead we consider the suggestion [50] that the uncertainty in the relative luminosities of different flavors must be in the range

$$\frac{1}{2} \leq \frac{L_{\nu_e}}{L_{\nu_x}} \leq 2 \quad ; \quad \frac{1}{2} \leq \frac{L_{\bar{\nu}_e}}{L_{\nu_x}} \leq 2 . \quad (25)$$

These limits in turn will put a constraint on the parameters $\phi_{\nu_e}^r$ and $\phi_{\bar{\nu}_e}^r$

$$\frac{1}{2} \frac{\langle E_{\nu_x} \rangle}{\langle E_{\nu_e} \rangle} \leq \phi_{\nu_e}^r \leq 2 \frac{\langle E_{\nu_x} \rangle}{\langle E_{\nu_e} \rangle} \quad ; \quad \frac{1}{2} \frac{\langle E_{\nu_x} \rangle}{\langle E_{\bar{\nu}_e} \rangle} \leq \phi_{\bar{\nu}_e}^r \leq 2 \frac{\langle E_{\nu_x} \rangle}{\langle E_{\bar{\nu}_e} \rangle} . \quad (26)$$

In Table 3 we present the lower limits (ll) and upper limits (ul) of the initial relative fluxes for different spectrum models LL, G1 and G3.

Model	$\langle E_{\nu_e} \rangle$	$\langle E_{\bar{\nu}_e} \rangle$	$\langle E_{\nu_x, \bar{\nu}_x} \rangle$	$\phi_{\nu_e;ll}^r$	$\phi_{\nu_e;ul}^r$	$\phi_{\bar{\nu}_e;ll}^r$	$\phi_{\bar{\nu}_e;ul}^r$
LL	10	15	24	1.20	4.80	0.80	3.2
G1	12	15	18	0.75	3.00	0.60	2.4
G3	12	15	18	0.75	3.00	0.60	2.4

Table 3: The average energies, upper limits (ul) and lower limits (ll) of the initial relative flux for the models used.

To compare different flux models and study more of the parameter space we vary $\phi_{\nu_e}^r$ and $\phi_{\bar{\nu}_e}^r$ in the range [0.5,5.0] and [0.5,3.5] respectively, for all the models. We find that varying $\phi_{\nu_e}^r$ and $\phi_{\bar{\nu}_e}^r$ give rise to different possibility of final spectrum as discussed in [42]. In addition to that we check it for different initial spectrum models. Here it is notable that usually the initial spectrum models come with a fixed value of $\phi_{\nu_e}^r$ and $\phi_{\bar{\nu}_e}^r$ (see Table 1) but the main idea in this analysis is about varying $\phi_{\nu_e}^r$ and $\phi_{\bar{\nu}_e}^r$. So here by initial spectrum models (like LL, G1, G3) we mean the energy dependence (ζ_{ν_α}) and neutrino average energies ($\langle E_{\nu_\alpha} \rangle$) of the models. In what follows, we will see that for the Inverted Hierarchy (IH) the final spectrum is very sensitive to the values of $\phi_{\nu_e}^r$, $\phi_{\bar{\nu}_e}^r$ and the model of initial spectrum. Whereas for Normal Hierarchy (NH), the results are less dependent on these quantities. We will discuss the reasons for this behavior.

2.3.1 Probability and Flux: NH

As already discussed in [41, 42], large flux (luminosity) of ν_x can induce simultaneous swap in both neutrino and antineutrino sector for NH. In these cases initially the system is in an unstable equilibrium. As it evolves, it partially swaps the flavor in both neutrino as well as antineutrinos, to end up in a stable state. We further study this over different spectrum models and initial relative fluxes. For each of the different models we vary $\phi_{\nu_e}^r$ and $\phi_{\bar{\nu}_e}^r$ in the range [0.5,5.0] and [0.5,3.5] respectively. We find that for several choices of $(\phi_{\nu_e}^r, \phi_{\bar{\nu}_e}^r)$ there is simultaneous swap in

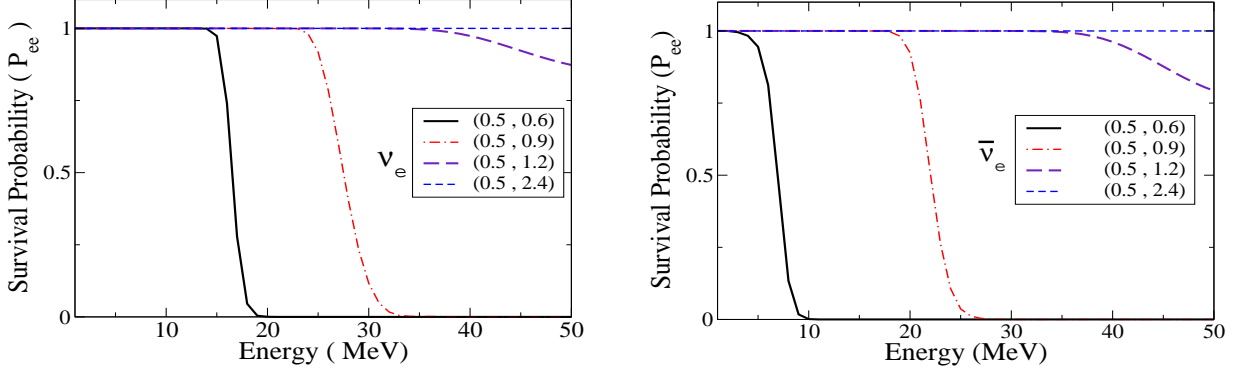


Figure 1: Survival probability for G3 spectrum in NH with different $(\phi_{\nu_e}^r, \phi_{\bar{\nu}_e}^r)$.

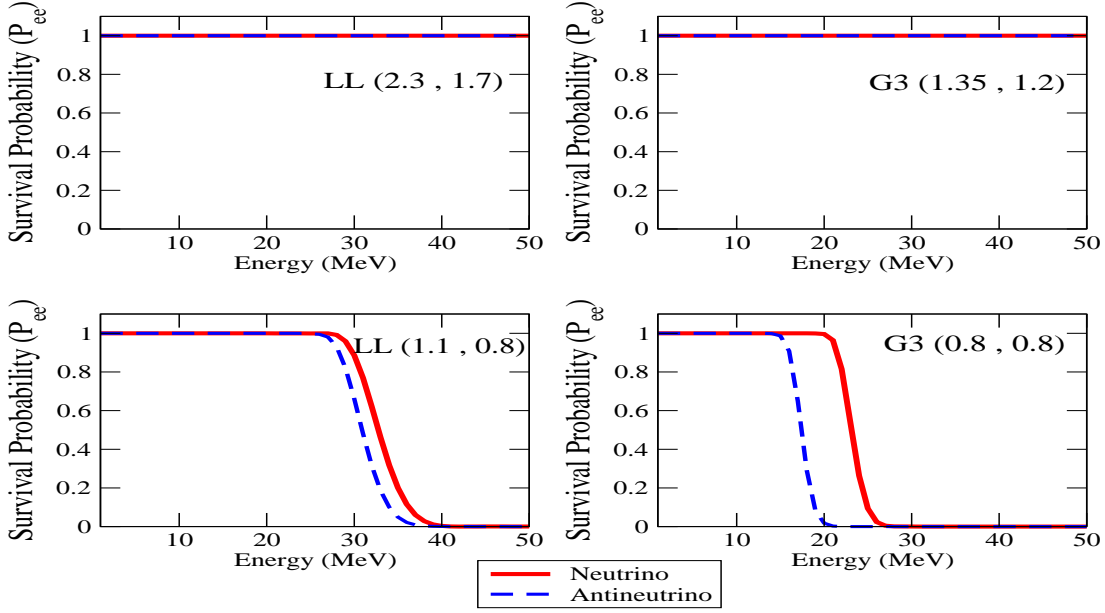


Figure 2: Survival probability for LL and G3 spectrum in NH with different $(\phi_{\nu_e}^r, \phi_{\bar{\nu}_e}^r)$.

both neutrino and antineutrino spectrum and this swap may generate prominent split in the final spectrum. For a specific model these split energies (E_c) may vary from low to high energies, depending on the value of $(\phi_{\nu_e}^r, \phi_{\bar{\nu}_e}^r)$.

Independent of the choice of spectrum models, these split features are seen for low values of $(\phi_{\nu_e}^r, \phi_{\bar{\nu}_e}^r)$, which implies large flux of ν_x compared to other flavors [42]. As the values of $(\phi_{\nu_e}^r, \phi_{\bar{\nu}_e}^r)$ increase the split energy (E_c) also increases and close to the equipartition point the split energy tends to infinity.

As an example see Figure 1 where survival probabilities are plotted for the spectrum G3. The left panel is for neutrino and right one for antineutrino. For a low value of $\phi_{\nu_e}^r$ (0.5), $\phi_{\bar{\nu}_e}^r$ is increased from 0.6 to 2.4 for both neutrino and antineutrino. From the figures it is evident that with this increment, split energies (E_c) also increase. For the same combination of $\phi_{\nu_e}^r$ and $\phi_{\bar{\nu}_e}^r$ the split energy is higher for neutrinos than for antineutrinos. We find these features are same for other

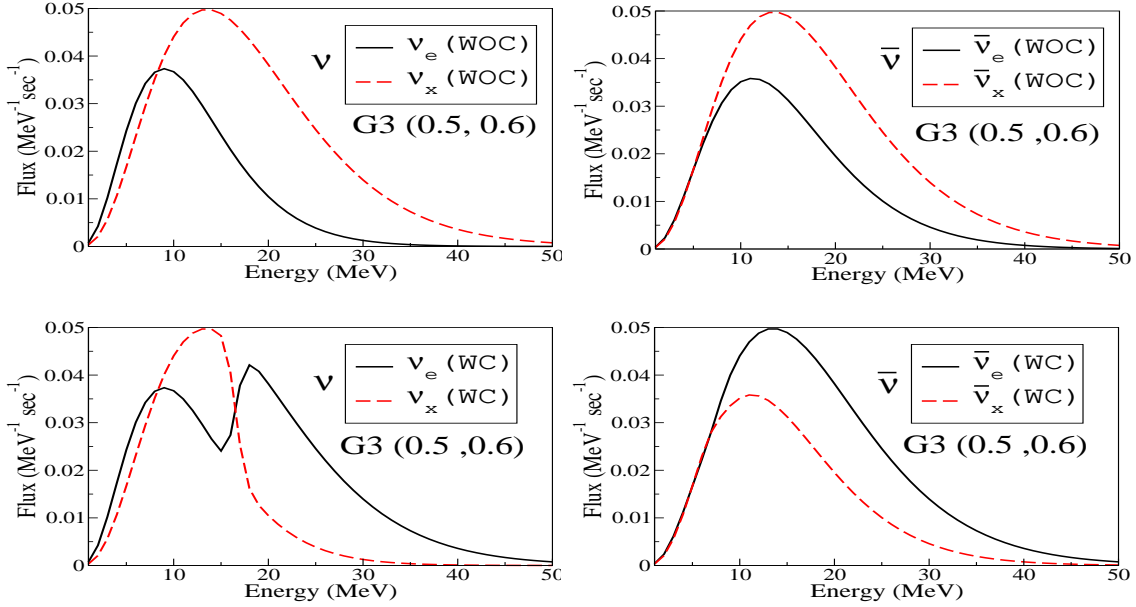


Figure 3: Flux for the different neutrino species for G3 with NH; WOC stands for “WithOut Collective” effects and WC for “With Collective” effects.

spectrum models too.

In Figure 2 we have shown the above mentioned features for LL and G3. The left panels are for LL and the right ones are for G3. The red straight lines are for neutrino and the blue dashed lines are for antineutrino. In the top panels the initial relative spectrum ($\phi_{\nu_e}^r, \phi_{\bar{\nu}_e}^r$) are chosen to be close to the equipartition point for both the models and for these values there is no split whereas for the lower panels ($\phi_{\nu_e}^r, \phi_{\bar{\nu}_e}^r$) are smaller and these panels show split for both neutrino and antineutrino sectors.

The flux corresponding to G3 and (0.5,0.6) are plotted in Figure 3. Left and right panels in this figure are respectively for neutrinos and antineutrinos. The upper panels are without collective effects (initial flux) and the lower ones are with collective effect (flux beyond collective region). The black lines in the panels are for electron type whereas the red dashed lines are for x-type. Clearly the lower panels show swap in both neutrino and antineutrino sector. The swap in both sectors are partial, that is, a part of the spectra below the “split energy” remains same. The antineutrino split feature is not clearly visible since E_c for them is low and the $\bar{\nu}_e$ and $\bar{\nu}_x$ fluxes are very close to each other at these energies. The probability plots for (0.5,0.6) in Figure 1 also show the low split energy for antineutrino. Note that the swap for neutrino spectra happens at a higher energy compared to the antineutrino spectra, this feature is also consistent with the probability plots in Figure 1.

2.3.2 Probability and Flux: IH

Probability and flux in the IH is much more complex and interesting than NH. Here also we vary the initial relative flux for different spectrum models and find wide variation of the final spectrum depending on the choice of ($\phi_{\nu_e}^r, \phi_{\bar{\nu}_e}^r$). These variations in spectrum with initial relative

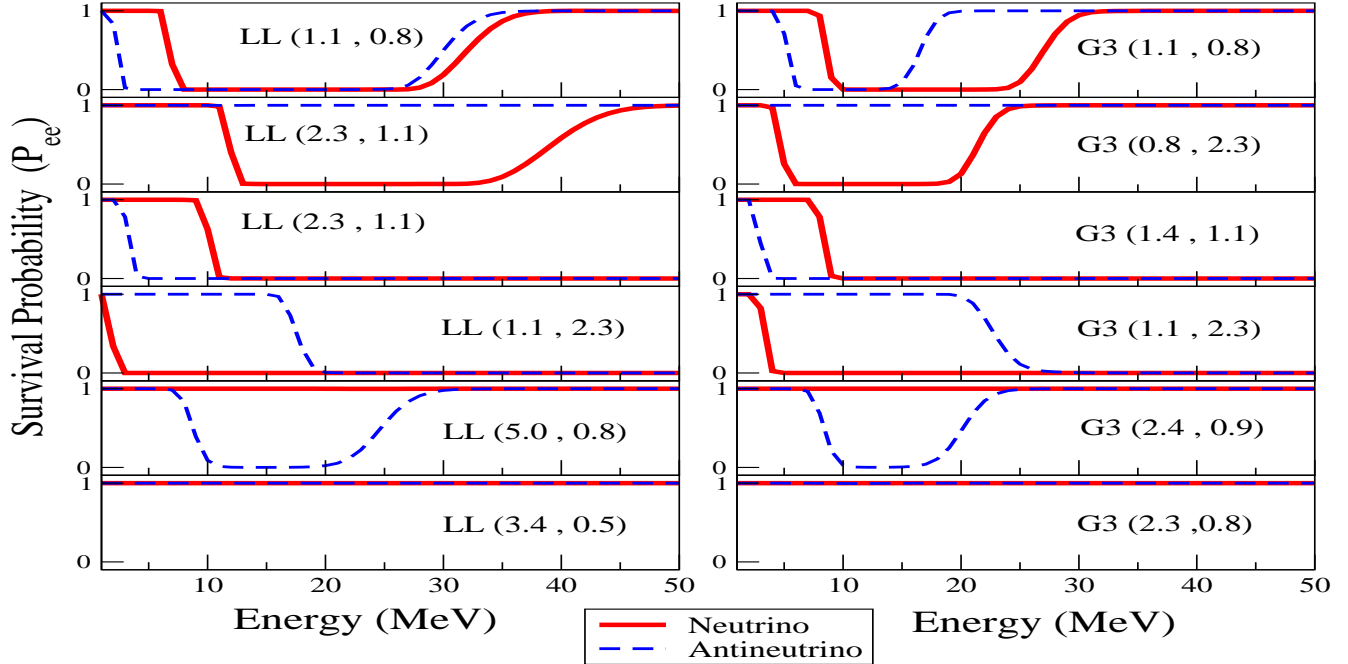


Figure 4: Survival Probability for LL and G3 spectrum in IH with different $(\phi_{\nu_e}^r, \phi_{\bar{\nu}_e}^r)$.

flux $(\phi_{\nu_e}^r, \phi_{\bar{\nu}_e}^r)$ have been attributed to meeting the instability condition of the initial system and adiabaticity violation [41] as well as to change of global initial condition with luminosity variation and minimization of potential energy [42]. We find that these changes in final spectrum are similar for different choices of spectrum models.

As discussed in [42], the different spectral features arise from the initial conditions, which may or may not lead the system to swap to minimize “potential energy”. We also find that in some cases the multiple swaps actually do take place but the swaps are so close that they can not be resolved numerically [41] and thus appear as if the swap or split features are absent. We find five spectral split patterns as mentioned in [42]. These five patterns are found for all three models of initial energy spectra LL, G1, G3. These are displayed (for LL and G3) in successive panels from top to bottom in Figure 5.

1. Dual split in both neutrino and antineutrino flux, say (II,II).
2. Dual split in neutrino but no split in antineutrino flux (II,0).
3. One split in both neutrino and antineutrino flux with the split energy of the neutrino higher than that of antineutrino (I,I)(H,L).
4. One split in both neutrino and antineutrino flux with the split energy of the neutrino lower than that of antineutrino (I,I)(L,H).
5. No split in neutrino but dual split in antineutrino flux (0,II).

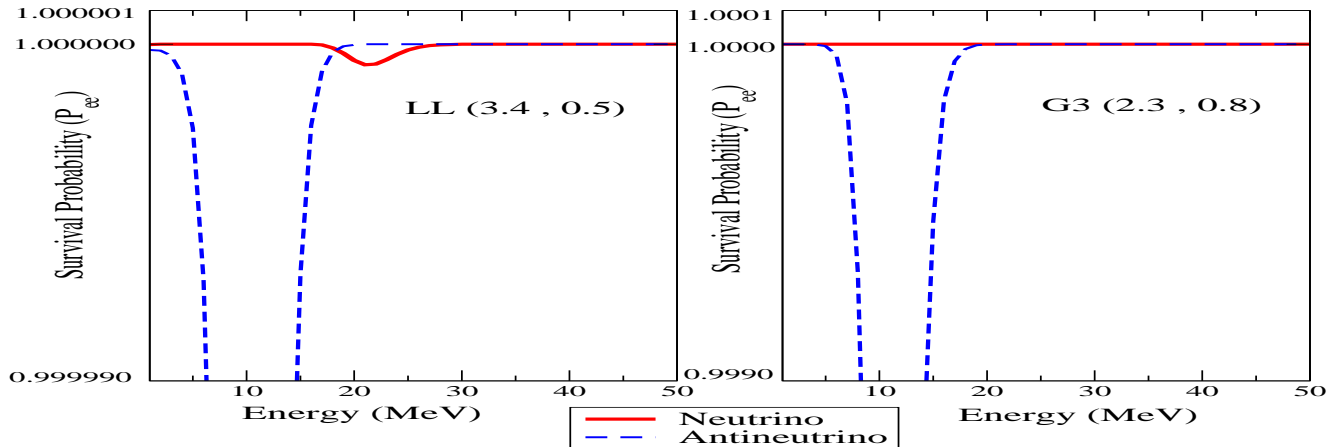


Figure 5: Survival Probability for LL (3.4, 0.5) and G3 (2.3, 0.8) spectrum in IH .

Apart from these five patterns we find a sixth possible pattern in which neither neutrino nor antineutrino show any swap in the spectrum. We call this (0,0). For this pattern (0,0) the effect of neutrino-neutrino interaction on both neutrino and anti neutrino flux is undetectable.

The physical reasoning behind the patterns in the top five panels are well explained [42] from the idea of potential energy minimization. Our analysis shows that in some sense all the different spectrum models are in the same footing as all of them give rise to similar split patterns with the change of initial relative flux or relative luminosity. As explained in [41] the basic feature is that there are multiple swaps or splits in both the neutrino and antineutrino sector but the swaps may disappear depending on the adiabaticity violation or it may be numerically unresolvable. Consider the new pattern, described in the lowest panel of Figure 4, where it seems that there is no swap in both neutrino and antineutrino sectors. When we study these cases carefully (Figure 5, left panel LL (3.4,0.5) and right panel G3 (2.3,0.8)) we find that they also show changes in survival probability similar to the other patterns. But the swaps here are incomplete and numerically undetectable. While in Figure 4 the change in probability for this case is visually unresolvable for all practical purposes, in Figure 5 it is visible, as we have increased the resolution.

For the fluxes we just give one example of the case (II,II) in Figure 6. Here we plotted the G3 neutrino spectrum in the left panel and the G3 antineutrino spectrum in right one. In both panels, the solid sky blue lines are for electron type without collective effect (WOC) and the solid red lines are for ν_x without collective effect (WOC). For the spectrum with collective effects (WC) dashed black lines are for electron type whereas dot-dashed blue lines are for ν_x . Here the spectrum model used is G3 and the initial relative fluxes are (1.1,0.8). We can see prominent dual split pattern in this flux figure as expected from the upper right panel of Figure 4.

Thus, depending upon the choice of initial relative fluxes ($\phi_{\nu_e}^r, \phi_{\bar{\nu}_e}^r$) the spectra can have different patterns, especially for IH. The possible values of ($\phi_{\nu_e}^r, \phi_{\bar{\nu}_e}^r$) can be in a wide range. Even if one assumes a factor-of-two-uncertainty in the relative luminosity [50], there can be considerable variations in the final flux characteristics. With so many possible patterns it will be really difficult to predict the initial relative neutrino fluxes, the energy distribution model and the extent of collective neutrino effect, even for a future galactic supernova event.

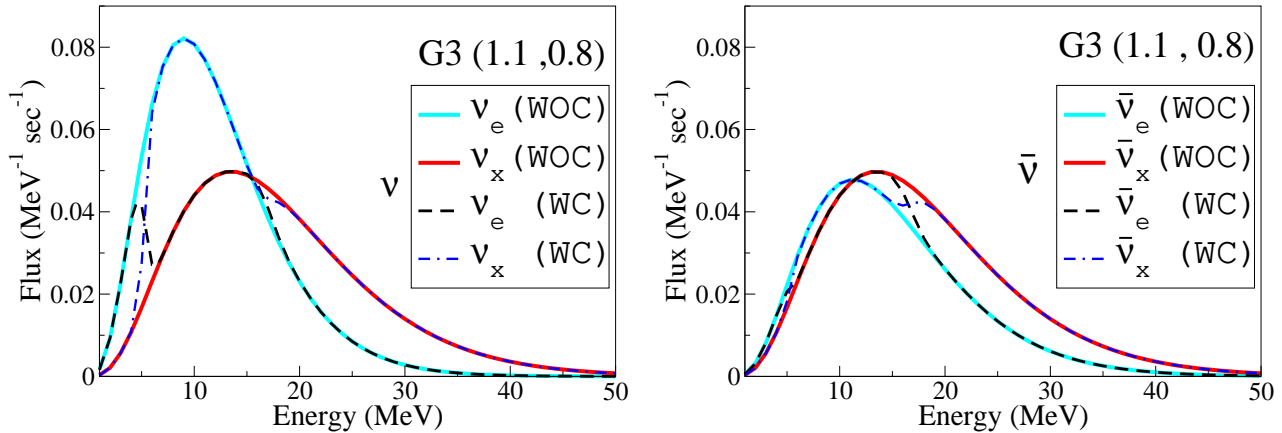


Figure 6: The neutrino and antineutrino fluxes for the model G3 with the relative luminosities (1.1,0.8), with and without collective effect for IH.

In the next section we discuss to what extent one can constrain the luminosities by demanding a neutron rich condition by the end of the collective region, required for successful r-process.

3 Neutrino Fluxes and r-Process Nucleosynthesis

In this section we discuss the effect of the flux of neutrinos radiated out in core collapse supernovae on the electron fraction and discuss the possibility of getting allowed regions for r-process nucleosynthesis and the resulting constraints on relative luminosities. As most simulations of core-collapse supernovae do not lead to explosions, there are uncertainties in the understanding of the late stage of the SN shock propagation. But the generally accepted scenario supported by simulations is that for iron core masses the shock wave gets initially stalled due to loss of energy through nuclear dissociation and then over timescale of a second, gets revived by the energy deposited by neutrinos radiating out, the so-called late-time neutrino heating mechanism leading to the delayed core collapse supernova [51]. This results in the development of a low density “hot bubble” region just behind the SN shock. The huge flux of neutrinos emitted from the proto-neutron star leads to the “neutrino-driven wind” which remains active for about 10 seconds after the core bounce. This creates neutron-rich regions of high entropy which are conducive to the development of the r-process. Different one dimensional delayed core-collapse SN calculations gave rise to different values for the entropy per baryon leading to conflicting conclusions about the r-process. However the ν -driven wind is still considered to be one of the most probable sites for the r-process [51].

The electron fraction i.e. the number of electrons (equal to the number of protons, due to charge neutrality) per baryon depends on the relative strengths of the reactions neutrino capture on neutrons and antineutrino capture on protons. So the evolution of Y_e as a function of radius as well as time needs to be determined carefully. Y_e can be expressed as [52]

$$Y_e = 1/(1 + \lambda_{\bar{\nu}_e p}/\lambda_{\nu_e n}) . \quad (27)$$

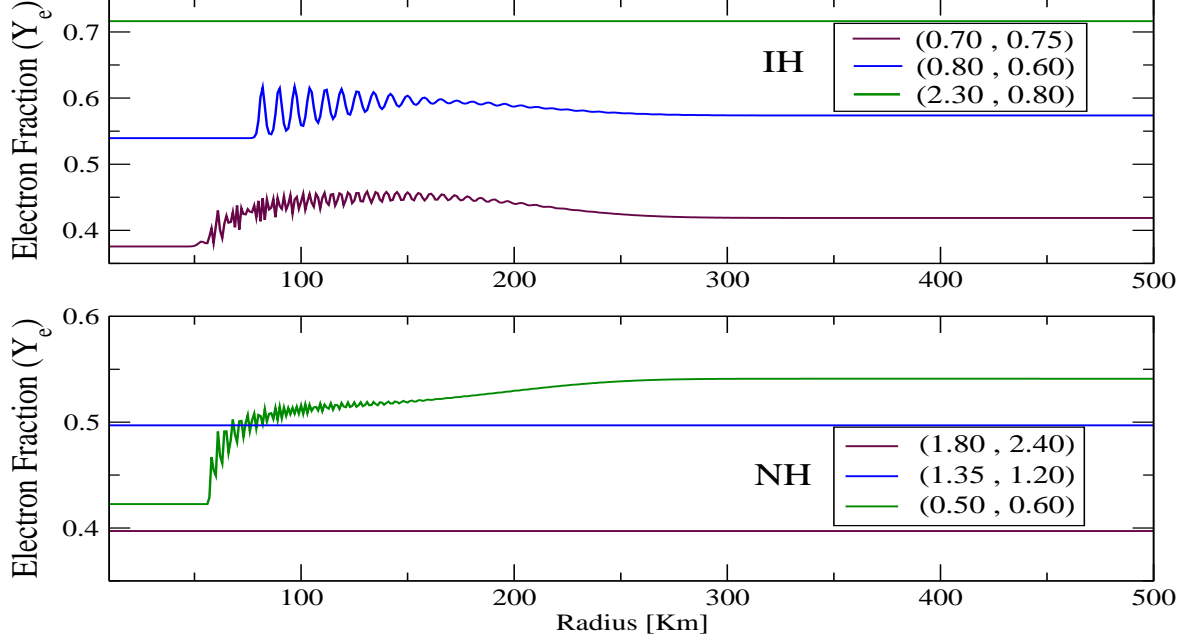


Figure 7: The electron fraction Y_e for both hierarchies as a function of ‘r’, the distance of the region from the center of the core. The spectrum model used is G3.

Where $\lambda_{\nu_e n}$ and $\lambda_{\bar{\nu}_e p}$ are the reaction rates for the reactions $\nu_e + n \rightarrow e^- + p$ and $\bar{\nu}_e + p \rightarrow e^+ + n$ respectively. Note that these reactions can in principle occur for both free and bound nucleons. However for the purpose of this work we will not consider the reactions on heavy nuclei. Thus,

$$\lambda_{\nu N} \approx \frac{L_\nu}{4\pi r^2} \frac{\int_0^\infty \sigma_{\nu N}(E) f_\nu(E) dE}{\int_0^\infty E f_\nu(E) dE}, \quad (28)$$

where $N = n$ or p and f_ν denotes the neutrino flux. The cross section used are

$$\sigma_{\nu_e n}(E_{\nu_e}) \approx 9.6 \times 10^{-44} \left(\frac{E_{\nu_e} + \Delta_{np}}{MeM} \right)^2 \text{ cm}^2, \quad (29)$$

$$\sigma_{\bar{\nu}_e p}(E_{\bar{\nu}_e}) \approx 9.6 \times 10^{-44} \left(\frac{E_{\bar{\nu}_e} - \Delta_{np}}{MeM} \right)^2 \text{ cm}^2, \quad (30)$$

where Δ_{np} the mass difference between neutron and proton is taken as 1.293 MeV [46]. For a detailed study of the effect of nuclear compositions on Y_e we refer to [16].

The minimal condition for the SN environment to become neutron rich is $Y_e < 0.5$ but a better condition for efficient r-process is to have $Y_e < 0.45$ or 0.4.

In [13, 46] the effect of collective neutrino oscillation on the electron fraction Y_e has been analyzed. Since the swap between the active neutrinos due to collective effect can change the n/p ratio, the r-process nucleosynthesis condition may also get effected. Again the r-process has to happen close to the supernova core as the baryon density would decrease very quickly from the core [46]. So we consider that r-process would happen at least within the collective region (400 km). It should be noted that since this analysis is for usual active neutrinos we need not consider MSW resonance as for such neutrinos the MSW resonance radius is very far (10^{4-5} km) from collective region (400 km). Thus r-process provide us with signatures of purely collective oscillations. For analysis of r-process with heavy ($\Delta m^2 = 10 eV^2$) neutrinos and collective effect see [13].

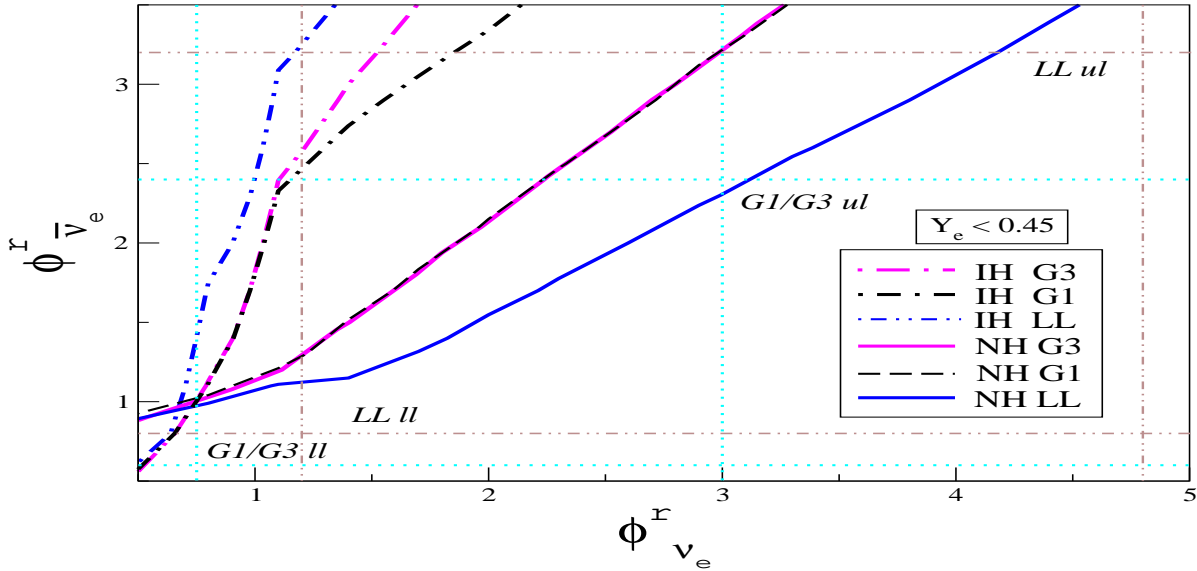


Figure 8: The exclusion plot consistent with $Y_e < 0.45$ for the spectrum G1, G3 and LL for both NH and IH. The allowed area is to the left of the curves. The dotted sky blue lines denotes the lower limit (*ll*) and upper limit (*ul*) of $\phi_{\nu_e}^r$ and $\phi_{\bar{\nu}_e}^r$ for G1 and G3, arising from the two fold degeneracy defined in Eq. (25). Similarly double dotted dashed brown lines denotes the *ll* and *ul* for the the spectrum model LL.

In section 2 it has been discussed how the choice of initial relative fluxes can give rise to wide possibilities in final neutrino and antineutrino flux due to collective effect. Thus for different choices of initial relative flux the final value of Y_e may change. We analyze the evolution of Y_e assuming different initial relative flux or luminosities. We also study these variations over different models of initial neutrino energy spectra (LL,G1,G3) and hierarchies (Normal and Inverted). To compare different spectra models we vary $\phi_{\nu_e}^r$ and $\phi_{\bar{\nu}_e}^r$ in the ranges (0.5,5.0) and (0.5,3.5) respectively (see Table 3).

The basic requirement of the neutron rich environment for r-process is primarily balanced by the reactions $\nu_e + n \rightarrow e^- + p$ and $\bar{\nu}_e + p \rightarrow e^+ + n$. The $\nu_e n$ reaction captures neutron whereas the $\bar{\nu}_e p$ adds neutron, so the increase of ν_e and $\bar{\nu}_e$ flux acts against and for neutron rich environment respectively. Thus a higher value of relative ν_e flux or $\phi_{\nu_e}^r$ with respect to relative $\bar{\nu}_e$ flux or $\phi_{\bar{\nu}_e}^r$

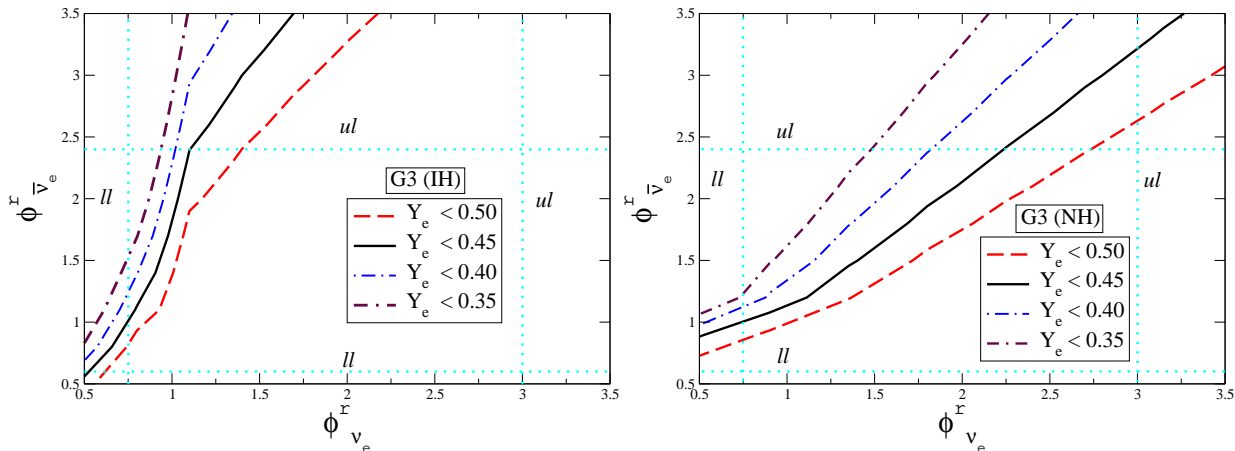


Figure 9: Exclusion plots for NH and IH for model G3. The exclusion condition is varied from $Y_e < 0.35$ to 0.5. The dotted sky blue lines denotes the ‘ ll ’ and ‘ ul ’ of $\phi_{\nu_e}^r$ and $\phi_{\bar{\nu}_e}^r$ for the spectrum model G3. The allowed region is on the left side of the exclusion curves.

does not support a neutron rich environment and results in electron fraction greater than 0.5. With the increment of relative $\bar{\nu}_e$ flux or $\phi_{\bar{\nu}_e}^r$ the electron fraction starts decreasing.

For example consider Figure 7. Here we study Y_e with the variation of relative luminosities for both NH and IH for the model G3. The figure shows the variation of Y_e with radius for different choices of luminosities. The top panel is for IH. The figure shows that, lower the relative luminosity of the neutrinos with respect to relative luminosity of the antineutrinos, lower is the electron fraction. For example consider the maroon lines for (0.70,0.75) and the blue lines for (0.8,0.6) in the upper panel for IH. Here as we decrease $\phi_{\bar{\nu}_e}^r$ from 0.75 to 0.6 and increase $\phi_{\nu_e}^r$ from 0.70 to 0.80 the electron fraction increases. If one increases $\phi_{\nu_e}^r$ further and reduces $\phi_{\bar{\nu}_e}^r$ then the electron fraction is even higher as is shown by the green curve [IH (2.3,0.8)]. Note that for the combinations of relative luminosities [IH (2.3,0.8)] in this curve there was no observable change in survival probability due to collective effect (see Figure 4) and hence the Y_e maintains a constant value. For the two other combinations in IH, the figure shows that Y_e exhibits fast oscillations within the first 200 km, which can be attributed to the bipolar collective oscillations. Beyond 300 km the value of Y_e approaches a fixed value [46] as the neutrino density decreases very fast and the collective effects end.

The lower panel shows the evolution of Y_e with radius for NH and G3 initial spectra. For the combination (0.5,0.6) the probability figure demonstrated the occurrence of collective effects and this gives rise to the oscillatory feature in Y_e . Due to collective effects the Y_e becomes more than 0.5 in this case. For (1.35,1.2) Figure 2 showed that there are no visible collective oscillation effect and so the Y_e stays constant. In the case of (1.8,2.4) relative luminosities of antineutrinos $\phi_{\bar{\nu}_e}^r$ is increased further and Y_e reduces below 0.45 which is required for successful r-process nucleosynthesis.

It is therefore clear that depending on the relative luminosities, Y_e can vary over a range of values some of which will not satisfy the requirement of successful r-process nucleosynthesis. Thus if we impose the condition that $Y_e < 0.45$ at the end of collective region (400 km) for the

occurrence of r-process then it constrains the luminosities. In Figure 8 we show the exclusion plot in the $\phi_{\nu_e}^r - \phi_{\bar{\nu}_e}^r$ plane corresponding to various values of Y_e . Here we plot exclusion curves for both IH and NH for all the three spectra models. The allowed area is to the left side of the curves. It is evident from the figure that the allowed region is more constrained for IH, since the effect of collective oscillations were more pronounced for IH.

It is clear that the lower we demand Y_e to be, the parameter space will be more constrained. Figure 9 shows the constraints for IH and NH for the model G3. The left panel is for IH and the right one for NH. Since higher values of $\phi_{\nu_e}^r$ gives higher Y_e as one reduces the required value of Y_e , $\phi_{\nu_e}^r$ gets more constrained. The constraint on $\phi_{\bar{\nu}_e}^r$ is relatively weak. But very low values of $\phi_{\bar{\nu}_e}^r$ are not allowed as we have seen that lower values of $\phi_{\bar{\nu}_e}^r$ increases the electron fraction.

We would like to point out here that the plots presented show the allowed fluxes for which one gets neutron-rich regions for r-process in the neutrino driven wind. But other considerations of baryon density and entropy in these regions need to be studied.

4 Summary and Conclusions

Collective flavor oscillations driven by neutrino-neutrino interaction at the very high density region of core collapse supernovae control the emitted flux of neutrinos of different flavors. In the process one or more swaps of flavors for both neutrinos and antineutrinos take place depending on the initial neutrino flux and distributions. We study the phenomena of spectral splits and consequent flavor swaps for different models of neutrino spectrum, varying the relative luminosities of neutrinos and antineutrinos for both normal and inverted mass hierarchy. The effect of spectral splits is found to be more pronounced for inverted hierarchy and depending on the initial luminosities one can get single or dual splits in neutrinos and/or antineutrinos. For a specific choice of relative luminosity we also find a case for inverted hierarchy where the splits are not resolvable numerically and is akin to no spectral splits for all practical purposes. Single split patterns are also obtained for normal hierarchy for some choices of the luminosities. Next we consider the impact of the collective oscillations and the spectral splits on the electron fraction Y_e , which determines if the environment is neutron-rich and compatible with r-process nucleosynthesis or not. The minimal requirement for r-process is the electron-to-nucleon ratio $Y_e < 0.5$, but a more favorable condition may be $Y_e < 0.45/0.40$. We consider the flavor evolution reduced to an effective two flavor model with oscillation between ν_e and ν_x and their antiparticles. The oscillation parameters are chosen as $\Delta m^2 = 3 \times 10^{-3} \text{ eV}^2$ and a small effective mixing angle $\theta = 10^{-5}$ in agreement with realistic 1 – 3 mixing.

The electron fraction (Y_e) as a function of the radius of the core is calculated and it shows an oscillatory behavior in the bipolar region due to collective effects, before saturating to a constant value which depends on the initial luminosities and the pattern of flavor swap. Different models of neutrino energy distributions are used. For each of the distributions initial fluxes of different flavors are varied and constraints on the initial neutrino fluxes consistent with successful r-process nucleosynthesis are shown in exclusion plots for these initial neutrino fluxes.

The variation in the number of spectral splits with the variation in the luminosity give rise to different possibilities of neutrino and antineutrino spectrum at the detector. The constraints on luminosities obtained by ensuring r-process nucleosynthesis can provide additional inputs in narrowing down the possible patterns.

5 Acknowledgments

S. Chakraborty wishes to thank Basudeb Dasgupta for useful discussions and acknowledges hospitality at Physical Research Laboratory and Harish Chandra Research Institute during the development stage of this work. S. Choubey and S.G. acknowledges support from the Neutrino Project under the XIth plan of HarishChandra Research Institute. K.K acknowledges hospitality at Institute of Mathematical Sciences. K.K and S. Chakraborty acknowledge support from the projects ‘Center for Astroparticle Physics’ and ‘Frontiers of Theoretical Physics’ of Saha Institute of Nuclear Physics.

References

- [1] G. Raffelt, *Stars as Laboratories for Fundamental Physics* (U. of Chicago Press, Chicago, 1996), 664 pp.
- [2] A. Dighe, J. Phys. Conf. Ser. **136**, 022041 (2008).
- [3] L. Wolfenstein, *Phys. Rev.* **D34**, 969 (1986); S.P. Mikheyev and A.Yu. Smirnov, *Sov. J. Nucl. Phys.* **42(6)**, 913 (1985); *Nuovo Cimento* **9c**, 17 (1986).
- [4] G. L. Fogli, E. Lisi, A. Mirizzi, and D. Montanino, *Phys. Rev. D* **68**, 033005 (2003) [hep-ph/0304056].
- [5] B. Dasgupta and A. Dighe, *Phys. Rev. D* **75** (2007) 093002 [hep-ph/0510219].
- [6] S. Choubey, N. P. Harries and G. G. Ross, *Phys. Rev. D* **74**, 053010 (2006) [hep-ph/0605255].
- [7] G. L. Fogli, E. Lisi, A. Mirizzi and D. Montanino, *JCAP* **0606**, 012 (2006) [hep-ph/0603033].
- [8] A. Friedland and A. Gruzinov, [astro-ph/0607244].
- [9] S. Choubey, N. P. Harries and G. G. Ross, *Phys. Rev. D* **76**, 073013 (2007) [arXiv:hep-ph/0703092].
- [10] J. T. Pantaleone, *Phys. Lett. B* **287**, 128 (1992).
- [11] G. Sigl and G. Raffelt, *Nucl. Phys. B* **406**, 423 (1993).
- [12] V. A. Kostelecky and S. Samuel, *Phys. Rev. D* **52**, 621 (1995).
- [13] S. Pastor, G. G. Raffelt and D. V. Semikoz, *Phys. Rev. D* **65**, 053011 (2002).
- [14] Y. Y. Y. Wong, *Phys. Rev. D* **66**, 025015 (2002).
- [15] A. B. Balantekin and Y. Pehlivan, *J. Phys. G* **34**, 47 (2007).
- [16] G. C. McLaughlin, G. M. Fuller and J. R. Wilson, *Astrophys. J.* **472**, 440 (1996) [arXiv:astro-ph/9701114].

- [17] S. Pastor and G. Raffelt, Phys. Rev. Lett. **89**, 191101 (2002).
- [18] R. F. Sawyer, Phys. Rev. D **72**, 045003 (2005).
- [19] H. Duan, G. M. Fuller and Y. Z. Qian, Phys. Rev. D **74**, 123004 (2006).
- [20] H. Duan, G. M. Fuller, J. Carlson and Y. Z. Qian, Phys. Rev. D **74**, 105014 (2006). tay signed in
- [21] S. Hannestad, G. G. Raffelt, G. Sigl and Y. Y. Y. Wong, Phys. Rev. D **74**, 105010 (2006); Erratum ibid. **76**, 029901 (2007).
- [22] G. G. Raffelt and G. Sigl, Phys. Rev. D **75**, 083002 (2007).
- [23] A. Esteban-Pretel *et al.*, Phys. Rev. D **76**, 125018 (2007).
- [24] H. Duan, G. M. Fuller, J. Carlson and Y. Z. Qian, Phys. Rev. D **75**, 125005 (2007).
- [25] G. G. Raffelt and A. Yu. Smirnov, Phys. Rev. D **76**, 081301 (2007); Erratum ibid. **77**, 029903 (2008).
- [26] G. G. Raffelt and A. Yu. Smirnov, Phys. Rev. D **76**, 125008 (2007).
- [27] H. Duan, G. M. Fuller and Y. Z. Qian, Phys. Rev. D **76**, 085013 (2007).
- [28] H. Duan, G. M. Fuller, J. Carlson and Y. Z. Qian, Phys. Rev. Lett. **99**, 241802 (2007).
- [29] G. L. Fogli, E. Lisi, A. Marrone and A. Mirizzi, JCAP **0712**, 010 (2007).
- [30] G. L. Fogli *et al.*, Phys. Rev. D **78**, 097301 (2008).
- [31] H. Duan, G. M. Fuller, J. Carlson and Y. Z. Qian, Phys. Rev. Lett. **100**, 021101 (2008).
- [32] B. Dasgupta, A. Dighe, A. Mirizzi and G. G. Raffelt, Phys. Rev. D **77**, 113007 (2008).
- [33] B. Dasgupta and A. Dighe, Phys. Rev. D **77**, 113002 (2008).
- [34] H. Duan, G. M. Fuller and Y. Z. Qian, Phys. Rev. D **77**, 085016 (2008).
- [35] B. Dasgupta, A. Dighe and A. Mirizzi, Phys. Rev. Lett. **101**, 171801 (2008).
- [36] A. Esteban-Pretel *et al.*, Phys. Rev. D **78**, 085012 (2008).
- [37] B. Dasgupta, A. Dighe, A. Mirizzi and G. G. Raffelt, Phys. Rev. D **78**, 033014 (2008) [arXiv:0805.3300].
- [38] J. Gava and C. Volpe, Phys. Rev. D **78**, 083007 (2008).
- [39] G. G. Raffelt, Phys. Rev. D **78**, 125015 (2008).
- [40] G. Fogli, E. Lisi, A. Marrone and I. Tamborra, JCAP **0904**, 030 (2009) [arXiv:0812.3031 [hep-ph]].

- [41] B. Dasgupta, A. Dighe, G. G. Raffelt and A. Y. Smirnov, Phys. Rev. Lett. **103**, 051105 (2009) [arXiv:0904.3542 [hep-ph]].
- [42] G. Fogli, E. Lisi, A. Marrone and I. Tamborra, arXiv:0907.5115 [hep-ph].
- [43] S. Chakraborty, S. Choubey, B. Dasgupta and K. Kar, JCAP **0809**, 013 (2008) [arXiv:0805.3131 [hep-ph]].
- [44] C. Lunardini Phys. Rev. Lett. **102**, 231101 (2009) [arXiv:0901.0568 [astro-ph.SR]]
- [45] H. Duan and James P Kneller J. Phys. **G36**, 113201 (2009). [arXiv:0904.0974 [astro-ph.HE]]
- [46] A. B. Balantekin and H. Yuksel New J. Phys. **7**, 51 (2005). [astro-ph/0411159]
- [47] T. Totani, K. Sato, H. E. Dalhed, J. R. Wilson, Astrophys. J. 496,216 (1998) [astro-ph/9710203],
- [48] T. A. Thompson, A. Burrows, P. Pinto, Astrophys. J. 592,434 (2003). [astro-ph/0211194]
- [49] M. T. Keil, G. G. Raffelt and H. T. Janka, Astrophys. J. **590**, 971 (2003) [arXiv:astro-ph/0208035].
- [50] C. Lunardini and A. Yu. Smirnov, JCAP **0306**, 009 (2003) [hep-ph/0302033].
- [51] For a recent review M. Arnould, S. Goriely and K. Takahashi, Phys. Rep.**450** 97-213 (2007).
- [52] Y. Z. Qian, G. M. Fuller, G. J. Mathews, R. Mayle, J. R. Wilson and S. E. Woosley, Phys. Rev. Lett. **71**, 1965 (1993).